Materials Chemistry and Physics 244 (2020) 122698

Contents lists available at ScienceDirect

Materials Chemistry and Physics

journal homepage: www.elsevier.com/locate/matchemphys

Enhancing the voltage and discharge times of graphene supercapacitors depositing a CNT/V_2O_5 layer on their electrodes

A.I. Mtz-Enriquez [a], C. Gomez-Solis [b], A.I. Oliva [c], A. Zakhidov [d], P.M. Martinez [d], C.R. Garcia [e], A. Herrera-Ramirez [b], J. Oliva [f,*]

[a] Cinvestav IPN, Unidad Saltillo, Parque Industrial, Ramos Arizpe, Coahuila, 25900, Mexico
[b] Universidad de Guanajuato, División de Ciencias e Ingenierías, 37150, León, Guanajuato, Mexico
[c] Cinvestav IPN, Unidad Mérida, Depto. de Física Aplicada, A.P. 73-Cordemex, 97310, Mérida, Yucatán, 97310, Mexico
[d] NanoTech Institute, The University of Texas at Dallas, Richardson, TX, 75080, USA
[e] Facultad de Ciencias Físico-Matemáticas, Universidad Autónoma de Coahuila, 25000, Saltillo, Coahuila, Mexico
[f] CONACYT-División de Materiales Avanzados, Instituto Potosino de Investigación Científica y Tecnológica A. C., 78216, San Luis Potosí, SLP, Mexico

HIGHLIGHTS

- Flexible Supercapacitors (SCs) were made with graphene electrodes.
- The SCs with CNTs and V^{4+}-VO defects in their electrodes had prolonged discharge times.
- A maximum constant voltage discharge of 0.38 V was observed for 10 h.

GRAPHICAL ABSTRACT

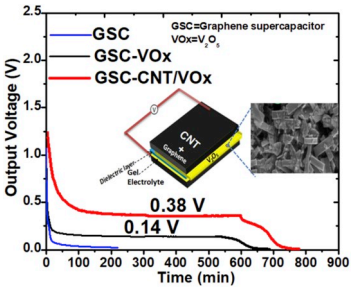

ARTICLE INFO

Keywords:
Graphene
V_2O_5
CNTs
Solid electrolyte
Supercapacitor

ABSTRACT

This work reports the electrochemical properties of graphene supercapacitors that employ flexible graphene electrodes (FGEs) coated by V_2O_5 (VOx) or carbon nanotubes (CNTs)/VOx layers. According to scanning electron microscopy images, the morphology of VOx consists in micro-ribbons with lengths of 20–45 μm and widths from 5 to 12 μm. The CNTs form interconnected long fibers, which were functionalized with carboxylic groups for producing defects. We demonstrated that the gel electrolyte used for the supercapacitors produces V^{4+}-oxygen vacancies (VO) defects. Both, the CNTs and V^{4+}-VO defects act as redox centers, which delay the current discharge in the supercapacitors. The presence of the carboxylic groups, defects in CNTs, defects in VOx, and oxidation states (V^{4+} and V^{5+}), were confirmed by the UV–Vis, XPS, and FTIR techniques. The electrochemical characterization of the supercapacitors indicated that the devices made with FGEs coated by VOx or CNTs/VOx layers produced constant voltages of 0.14 V and 0.38 V during 535 and 593 min, respectively. The increase of voltage is explained by the increase of surface area and by the extra redox centers (defects) introduced by the CNTs. The results indicated that the CNTs/VOx layer increases the voltage and discharge times of the graphene supercapacitors, which can be of interest for the development of graphene systems with high charge storage capabilities.

* Corresponding author.
E-mail address: jroliva@conacyt.mx (J. Oliva).

https://doi.org/10.1016/j.matchemphys.2020.122698
Received 1 November 2019; Received in revised form 15 January 2020; Accepted 20 January 2020
Available online 23 January 2020

1. Introduction

Currently, industry and scientific communities are looking for inexpensive sources of energy such as hydrogen (which can be generated by electrocatalysis using efficient materials such as porous W-doped CoP nanoflakes and WSe_2 semiconductor [1,2]) and for efficient energy storage devices with high mechanical properties (flexibility and stretchability). Energy storage devices with these characteristics would motivate the development of wearable electronics products such as flexible sensors, bendable cell phones, and flexible displays [3]. Actually, lithium ion batteries (LIBs) and electrochemical supercapacitors are the forefront technologies to provide energy for wearable or portable devices [4]. However, the main issues of the LIBs are flammability, shortage of the Li component, dendritic lithium short circuit, relatively high cost, and thermal instability after long periods of operation, among others [5]. For supercapacitors, the main problems are: i) their performance depends on the surface area of the electrode, pore size, and the electrical conductivity; ii) they have a short discharge time; and iii) they have lower energy densities than LIBs [6]. In order to solve these problems, other technologies have emerged like graphene/carbon nanotubes (CNTs) based batteries/supercapacitors (SCs), which have superior properties such as flexibility, compact size, being lightweight and environmentally friendly, and having fast charge-discharge and higher cycling [3,7]. Particularly, graphene has attracted attention because it can be doped with a rich-electron organic molecular such as Polyethylenimine (PEI) to improve the stability of graphene field effect transistors (GFETs) [8] or to make efficient electrodes for SCs. For example, Zang et al. [9] fabricated thin-film supercapacitors that use graphene woven-fabric (GWF) films as electrode materials. The GWF films were synthesized by using chemical vapor deposition on copper mesh. This device presented an specific capacitance of (267 F/g) and 100% of capacitance retention after 1,000 charge/discharge cycles. Ervin et al. [10] printed graphene electrodes on Kapton tape, obtaining a maximum specific capacitance of 192 F/g and a power density of 10 kW/kg. Gao et al. [11] reported a solid state supercapacitor with low cost and environmentally-friendly electrodes made of cellulose fibers decorated with reduced graphene oxide (rGO), which reached a high capacitance of 207 F/g and capacitance retention of 99% after 5,000 charge/discharge cycles. Also, SCs made with graphene and activated carbon reached a maximum capacitance of 59 F/g and power density energy of 65 kW/kg [12]. The capacitance retention of this device was 95% after 10,000 cycles. Furthermore, thick electrodes of graphene (400 μm) have been employed to fabricate planar SCs with specific efficiencies as high as 172 F/g [13]. Additionally, CNT based SCs have been reported to improve the stretchability and flexibility of supercapacitors. Some electrodes used to fabricate those devices are CNTs/Polyanine (PANI), CNTs/polyimide (PI), RuO_2@CNTs, or CNTs/MnO_2 [14–17]. The conductive polymers PANI and PI provide better flexibility properties to the CNTs' electrode, while the RuO_2 and MnO_2 are used to enhance the electrochemical performance of the supercapacitors by pseudocapacitive effects [15–17]. Energy densities of 100–300 Wh/kg and specific capacitances of 100–320 F/g are reported for these CNT based SCs. Although the mentioned graphene/CNT based energy storage devices present high specific capacitances and high electrochemical stability, they present various problems such as complex, long, and expensive procedures for fabricating their electrodes or deficient encapsulation, which could cause the corrosive electrolyte to leak. Moreover, their charge times are similar to the discharge times; therefore, their charge/discharge profiles have a triangular shape. This is a disadvantage because longer times (20–150 min) are required to complete the charge. Due to the last problems, energy storage devices with the following characteristics are still required: fast charging time, long discharge time, easy fabrication process, and low cost.

As an effort to fabricate graphene based energy storage devices at low cost, some groups have employed vanadium pentoxide (V_2O_5) based electrodes, an inexpensive and abundant thermochromic material which facilitates the intercalation-desintercalation of Li^+ ions [18,19]. Therefore, V_2O_5-graphene nanocomposites, Na-V_2O_5-graphene nanocomposites, and V_2O_5 cryogel/graphene nanosheet composites have been used as cathode materials to enhance the performance in LIBs/Na based batteries [18,20–22]. Moreover, V_2O_5 is a promising candidate for electrode material because of its high theoretical capacitance of 2120 F/g [23]. Several works about graphene electrodes containing V_2O_5 have been reported: Ahirrao et al. [24] synthesized a composite made of V2O5 nanowires and graphene oxide (V2O5 NW-rGO), which was studied as electrode material using a three electrode configuration (the electrolyte used in the cell was 1 M $NaSO_3$). They reported a maximum capacitance of 1002 F/g (at 1 A/g), energy density of 116 Wh/kg, power density of 1520 W/kg, and capacitance retention of 83% after 5,000 cycles. Furthermore, Lee et al. [25] evaluated the electrochemical performance of an electrode made of V2O5 nanowires and rGO for the same number of cycles and obtained similar capacitance retention (82%) but lower capacitance (288 F/g). Furthermore, Liu et al. [23] fabricated a hybrid aerogel composite electrode made of V2O5 nanospheres and graphene sheets (rGO/V2O5) and found a maximum specific capacitance of 384 F/g (at 1 A/g) and energy density of 80.4 Wh/kg. In this work, the electrolyte employed was 1 M $LiClO_4$/PC (propylene carbonate). If the rGO/V2O5 electrode is mesoporous, a capacitance of 384 F/g was obtained in 1 M $NaSO_3$ electrolyte [4]. In addition, Saravanakumar et al. [26] fabricated an interconnected V2O5 nanoporous network and studied its electrochemical performance in K_2SO_4 aqueous electrolyte for SCs applications. They state that the introduction of a nanoporous network enhanced the ion diffusion and reached a capacitance of 316 F/g and an energy density of 43.8 Wh/kg. Finally, Xu et al. [27] reported a maximum capacitance of 195 F/g (at 1 A/g) for graphene/V2O5 xerogels nanocomposites.

Although the SCs based on V2O5 mentioned above have demonstrated good values of capacitance and power densities, they still have low energy density values due to their fast discharge times (150–5,000 s), which limit their use as batteries for portable devices. Additionally, these V2O5 (VOx) based electrodes/supercapacitors require sophisticated and long procedures of synthesis (hydrothermal, precipitation, and solvothermal) methods, which are not appropriate for mass production. Due to these disadvantages, an easy method to fabricate a graphene + CNT/VOx composite electrode is proposed. This electrode was later used to make flexible graphene SCs with long discharge times. The novelty of this work is the fact that the graphene + CNT/VOx electrodes contained carboxylic groups/defects which worked as redox centers, this in turn, provided a high storage capacity to the SCs. The discharge time of these SCs was at least 10 h. If the SCs are made without CNTs, their discharge times are short, as previously reported VOx based SCs. The surface, chemical, and morphological analysis of the graphene + CNT/VOx composite electrodes was discussed to understand the high storage capacity of the SCs made with these electrodes.

2. Experimental section

2.1. Synthesis of flexible graphene electrodes and V_2O_5 microbelts

The flexible graphene electrodes (FGEs) were fabricated using a molding/casting method previously reported in Ref. [28]. The V_2O_5 microbelts were synthesized using a hydrothermal method reported by Qin et al. [29] but we carried out some modifications. In a typical synthesis, we dissolved the ammonium metavanadate (Sigma Aldrich, purity 99%) in water to obtain a 1 M aqueous solution (solution A). Afterwards, 10 ml acetic acid glacial (Sigma Aldrich, purity 98.5%) was added to 90 ml of solution A and we obtained solution B with volume of 100 ml. Next, the solution B was put in a Teflon-lined stainless autoclave and was subjected to a hydrothermal treatment at 180 °C for 24 h. After this time the autoclave was cooled down and a yellow-orange powder was observed at the bottom part of the autoclave. This powder was removed and washed with water and ethanol several times. Finally, the

powder was grinded to obtain fine particles.

2.2. Device fabrication

In a typical procedure, the graphene supercapacitors were made as follows: First, slurry was prepared by mixing PMMA, V_2O_5 (VOx), methanol, and acetone using 0.5:0.3:1:1 wt%, respectively. Second, a piece of FGE (1 cm × 1 cm) was coated with the mixture and dried for 30 min at 80 °C. Subsequently, a semipermeable acrylate polymer membrane (APM) with 100 μm of thickness was sandwiched between the two FGEs (one of them coated with slurry made of VOx) and hot pressed with 0.1 ton. Afterwards, the FGEs were externally connected with copper wires and encapsulated. Another device was fabricated using a FGE which had CNTs on its surface (the CNTs layer was manually deposited on the FGE using a manual transfer technique). These CNTs were synthesized using the chemical vapor deposition method reported by Lepro et al. [30]. The FGE + CNT electrode was also coated with the slurry made of VOx and this device was finished using the procedure mentioned above. It is worthy to mention that the FGE + CNT electrode was subjected to an acid treatment (before its use to make the SCs) employing the procedure previously reported by Singh et al. [31] with some modifications: First, the FGE + CNT electrode was immersed in 30 ml of concentrated nitric acid (sigma Aldrich, 70%), later, the acid + electrode was put into a glass vial and this was heated at 70 °C for 12 h under magnetic stirring. Subsequently, the FGE + CNT was removed from the vial, washed with water and ethanol several times and finally dried at 110 °C for 3 h in air using a hot plate. All of the devices contained a gel electrolyte made of PMMA, acetone, water, and phosphoric acid (70% conc.). For all the SC devices, their anodes contained VOx, CNTs or combinations of these materials while their cathodes were only the bare FGEs. The gel was included between the APM and the FGE without the slurry coating (cathode). Thus, three graphene SCs devices were studied in this work: one without VOx, the second one included the VOx layer on its anode, and the third one included the CNTs/VOx layer on its anode. These devices are referred from here as GSC, GSC-VOx and GSC-CNT/VOx, respectively.

2.3. Electrode and device characterization

The electrodes' surface was analyzed using scanning electron microscopy (SEM Quanta 250), and the X-ray diffraction patterns (XRD) were obtained using a Bruker D8 equipment. X-ray photoelectron spectroscopy (XPS) spectra were recorded by using Thermo Scientific K-Alpha Spectrometer equipment. The Fourier transform infrared (FTIR) and absorbance spectra of electrodes were recorded with Perkin Elmer equipment. Finally, the cyclic voltammetry (C-V) and galvanostatic charging/discharging (GCD) curves for the SCs were recorded using an electrochemical station (Galvanostat/Potentiostat Wavenow) with a two-electrode configuration. The C-V curves were recorded using a scan rate of 70 mV/s. Electrochemical impedance spectroscopy experiments were carried out using a Biologic SP-300 galvanostat/potentiostat. For the two electrode configuration employed in this work, the specific gravimetric capacitance was calculated from the galvanostatic discharge curves using:

$$C_s = \frac{2I\int V(t)dt}{m\left(\Delta V^2\right)} \quad (1)$$

where I is the discharge current, $\int V(t)dt$ is the total area under the discharge curve, m the total mass of both electrodes and ΔV represents the potential change after a full discharge.

The specific energy density (E) in Wh/kg and specific power density (P) in W/kg of the flexible supercapacitors were evaluated from the charge-discharge curves using the equation:

$$E = \frac{1}{2}\left[\frac{C_s \cdot \Delta V^2}{3.6}\right] \quad (2)$$

It is worth mentioning that all the experimental curves for the graphene SCs characterized in this work were obtained by averaging the results of four devices.

3. Results and discussion

3.1. Structure and morphology

The electrodes employed for the fabrication of the SCs were characterized to understand the role of the CNTs and VOx microstructures on their electrochemical performance. It is worthy to mention that characterization of the bare FGEs in a previous report shows porous surfaces with pore sizes from 15 to 40 μm [28]. The SEM image in Fig. 1a shows the CNTs deposited on the FGEs, those are interconnected and form long CNT fibers. They resemble a textile and can be oriented in a preferential direction as reported in Ref. [30]. These CNTs are very strong mechanically (strength = 1040 MPa) [32], allowing them to stretch for easy deposition on any type of substrate (including FGEs). In addition, the CNTs have multi-wall structure and have an average diameter of 12 nm. Detailed TEM pictures and SEM images at higher magnification have reported previously in Ref. [30]. Fig. 1b depicts a SEM image of the CNTs layer deposited on the FGEs (FGE + CNTs electrode) where the surface of the FGEs below the CNTs is still visualized (see red circles), since the transmittance of the CNTs is at least 85% [32]. The presence of CNTs adds extra surface area to the FGE, which benefited the electrochemical properties of the GSC device, as explained later. Fig. 1c shows an image of the flat VOx micro-ribbons (with rectangular shape) employed for the fabrication of the GSC device. The VOx micro-ribbons presented lengths from 5 to 45 μm and widths from 2 to 12 μm. Some of them are broken or partially formed, see green circles. When these micro-ribbons are deposited on the FGEs (to form the FGE + VOx electrode), they randomly cover the surface of the huge graphene nanoplates (see yellow circles in Fig. 1d) or they are deposited into the pores of the FGEs (see blue circles), creating a very irregular and porous VOx layer on the FGEs. In the case of the FGE + CNTs/VOx electrode (FGE + CNTs coated with VOx microparticles), the VOx micro-ribbons can be located directly on the surface of the CNTs or be trapped into the network formed by the CNTs fibers (see red circles in Fig. 1e). Figs. S1, S3 and S4 in supporting information show other SEM images of the FGE + CNT, FGE + VO and FGE + CNT/VO electrodes to better visualize the distribution of CNT and VOx microparticles on the FGEs. Fig. S2 in supporting information showed the VOx microparticles at higher magnification to better observe their morphology. In general, the VOx and CNTs are not completely covering the surface of the FGEs, there are empty spaces (pores) and therefore, the layers of VOx and CNTs deposited on the FGEs are not uniform. The VOx and CNTs are only decorating the surface of the FGEs. Finally, Fig. 1f shows the general configuration of the SCs fabricated in this work. The upper electrode was made of FGE + CNT/VOx. The semipermeable APM is shown in the middle part of the sandwich (blue layer in Fig. 1f) and the gel electrolyte was put below it. The second FGE without CNT/VOx coating is located at the bottom of the device.

In order to confirm the crystalline nature of each type of electrode employed for the fabrication of the SCs, all the electrodes were analyzed using the XRD technique. Fig. 2a shows the diffraction patterns for the V_2O_5 powders with two main diffraction peaks at $2\theta = 15.5^\circ$ and 26.2°, which correspond to the (200) and (100) orientations, respectively. The VOx presents an orthorhombic structure according to the JCPDS 41-1426 card [27]. The XRD pattern of the bare FGE presents a broad shoulder centered at 19° and a peak at 26.6°, which are attributed to the acrylate polymer and to the presence of the graphene nanoplates used to fabricate the FGE [27,28], respectively. It is worthy to mention that the

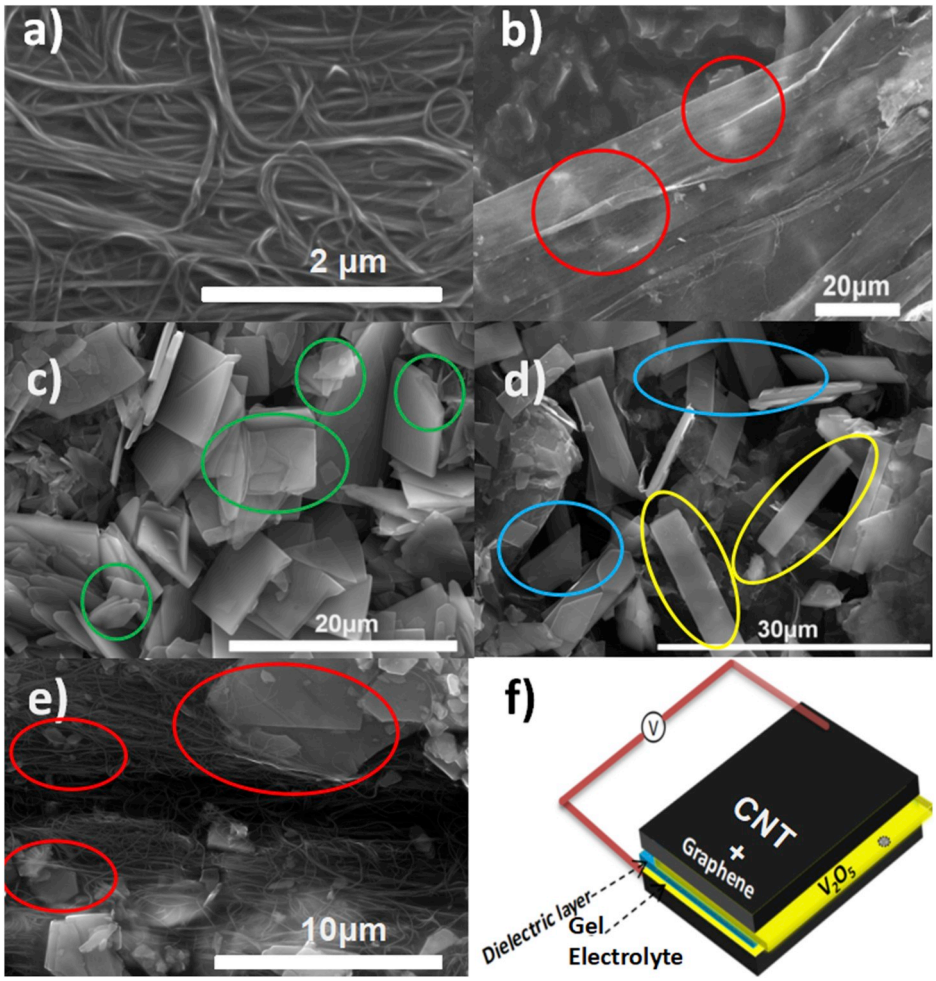

Fig. 1. SEM images of: a) bare CNT (50000x), b) FGE coated with CNTs (1000x), c) V_2O_5 powders (5000x), d) V_2O_5 powders deposited on the FGE (4000x), e) V_2O_5 powders attached to CNTs (12000x), and f) configuration of the flexible VOx based supercapacitors fabricated in this work.

graphene nanoplates employed to make the FGEs are formed by stacking 2-4 layers of single graphene [28], therefore, the (002) peak in Fig. 2a could also correspond to the graphite structure. Typically, the (002) peaks of graphene and graphite are in the same 2θ position [33]. When the VOx is added to the FGE, the XRD pattern again shows the broad band of the polymer; the peak associated to VOx at 12.5° and the very intense peak at 26.6° are attributed to the simultaneous presence of graphene and VOx. We believe that the peak at 26.6° contains the contribution of both materials because it is wider and more intense than that observed for the bare FGE, compare blue and black curves in Fig. 2a. Finally, the shift of the diffraction peak for VOx from 15.5° to 12.5° could be associated with scattering effects produced by the VOx microparticles located in the porosity of the FGEs [27].

3.2. Surface characterization of the FGE + CNT and FGE + CNT/VOx electrodes

The FGE + CNT electrode was functionalized with COOH groups (before its use to construct the SCs) using an acid treatment previously reported by Singh et al. [31]. Details for this acid treatment were mentioned in section 2.2. These functional groups will benefit the electrochemical properties of the SCs as will be explained in Section 3.3. The FTIR spectrum (red curve) in Fig. 2b confirms the presence of such groups. The broad peak from 2500 to at 3600 cm^{-1} is due to O-H stretching vibration of the hydroxyl groups and the 2855 cm^{-1} peak is assigned to the C−H stretching vibration of methylene produced by the defect sites of acid-oxidized MWCNT surface [31]. Also, the peak at 2327 cm^{-1} is associated with the O-H stretch from strongly hydrogen-bonded –COOH, while the peak at 1543 cm^{-1} is related to the carboxylate anion stretch mode [34]. Moreover, the peak at 1643 cm^{-1} is associated with the C═C, which confirms the bonding between the CNTs and graphene, while the broad band centered at 947 cm^{-1} is attributed to C-OH bonds [35]. The FTIR spectrum of the VOx powders presents a broad band centered at 3248 cm^{-1} which is attributed to the OH groups [36,37]. Additionally, the peaks centered at 529, 711, and 961 cm^{-1} correspond to the asymmetric/symmetric vibrations of V-O-V and V-O bonds, respectively [36,37]. When the VOx powder is deposited on the FGE + CNTs layer to form the FGE + CNT/VOx electrode, the same peaks of VOx are observed but their intensity was lower due to the smaller content of VOx (6 mg) on the FGE + CNTs electrode (compare blue and black curves in Fig. 2b).

3.3. Electrochemical performance of the supercapacitors

The current-voltage (C-V) curve corresponding to the GSC device was very thin, indicating a low capacitance, see blue curve in Fig. 2c. When the FGE + VOx electrode is employed in the SCs (GSC-VOx device), a broader C-V curve is observed (see red curve), indicating that VOx improves the capacitance. Inset in Fig. 2c provides details of the C-V curve for the GSC-VOx device. When the FGE + CNT/VOx electrode is employed in the SCs (GSC-CNT/VOx device), two shoulders (cathodic and anodic peaks at 0.42 V and 0.26 V, respectively) are clearly observed in the C-V curve, suggesting the presence of diffusion-controlled redox reactions [38]. Additionally, the C-V curve is wider

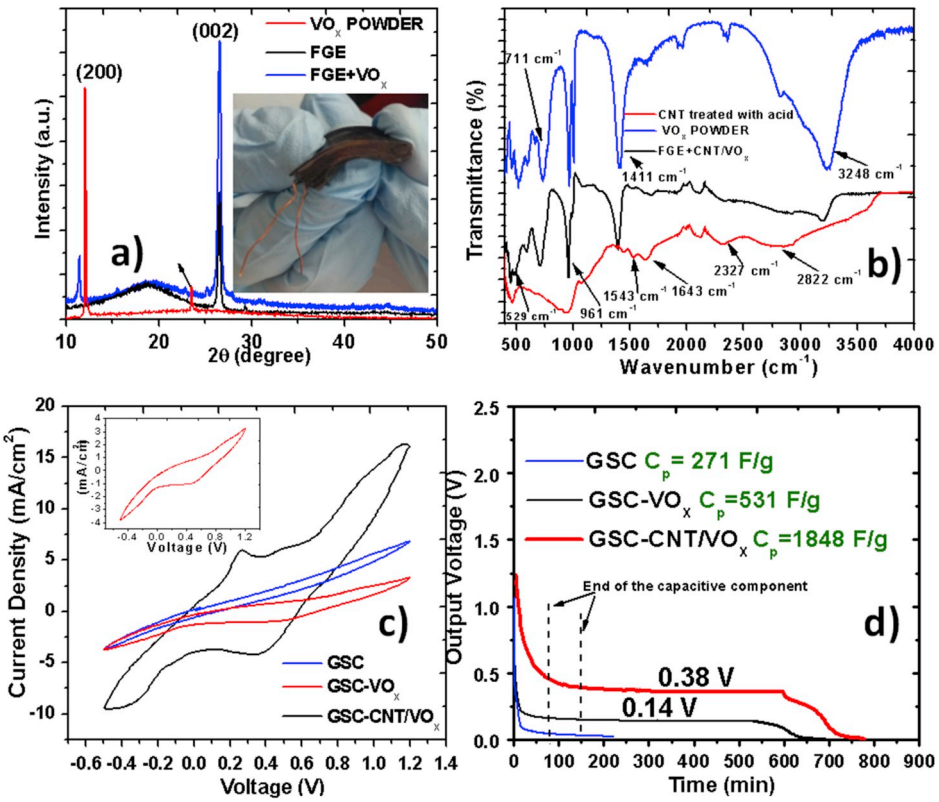

Fig. 2. a) XRD patterns of VOx powders, FGE and FGE + VOx electrode; b) FTIR spectra of CNTs treated with nitric acid, VOx powders and FGE + CNTs/VOx electrodes; c) C-V curves for the GSC, GSC-VOx and GSC + CNTs/VOx devices; and d) GCD curves for the GSC, GSC-VOx and GSC + CNT/VOx devices. Inset in Fig. 2a shows a picture of the flexible SC and inset in Fig. 2c shows a closer view of the C-V curve of the GSC-VOx device.

than that of the GSC-VOx device, and the maximum current value (at 1.2 V) increases due to the presence of CNTs. This probably occurs because the CNTs provide extra surface area to the FGE electrode, thus enhancing the capacity of the device for storing ions. Also, all the C-V curves show good capacitance even in the negative window (from 0 to −0.5 V), indicating that the change of polarity does not affect its performance. However, the capacitance value is achieved in the positive window from 0 to 1.2 V and a wide C-V curve with Faradaic peaks is observed. The most dramatic change is observed in the charge-discharge curves (see Fig. 2d). The GSC device discharges exponentially from 1.2 V to 0 V after only 214 min, while the GSC-VOx device presents an exponential decay voltage from 0 to 77 min; after this time, it remains constant at 0.14 V until 535 min. For the GSC-CNT/VOx device, the exponential discharge lasts from 0 to 148 min, with constant voltage at 0.38 V until 593 min. Previous reports indicate that the charge/discharge times in SCs are similar, which produces GCD curves with triangular shapes [14–17]. However, two components in the discharge profile for the GSC-VOx and GSC-CNT/VOx devices were observed. One was capacitive (exponential decay voltage) and the second one (the flat profile) was associated to the storage charge by a redox reaction diminishing the leakage current. Such constant output voltage was previously observed in graphene batteries [39]. The capacitance of the exponential component was calculated considering the mass of both electrodes. In the case of the GSC-VO device, the total mass for its electrodes was calculated as follows: 2 x (mass of FGE + mass of VOx). For the GSC-CNT/x device, the total mass for its electrodes was calculated as follows: 2 x (mass of FGE + mass of VOx + mass of CNT). The total masses used for the calculations of capacitance were: 57 ± 0.1 mg, 63 ± 0.1 mg and 66 ± 0.1 mg for the GSC, GSC-VOx and GSC-CNT/VOx devices, respectively. Capacitance values of 271, 531, and 1848 F/g (at 1 A/g) were obtained for the GSC, GSC-VOx and GSC-CNT/VOx devices, respectively. Also, the values of energy density were 54.2, 106.2, and 369.6 Wh/kg for the GSC, GSC-VOx and GSC-CNT/VOx devices, respectively. Those results are summarized in Table 1. The capacitance and energy density values for the GSC-CNT/VOx device are higher than these reported for other graphene/VO based materials with capacitive properties: VOx nanowires with reduced graphene oxide (1002 F/g and 116 Wh/kg) [24], graphene decorated VOx nanobelts (288 F/g) [25], rGO/VOx nanoparticles (384 F/g and 80.4 Wh/kg) [23], pure VOx nanoporous network (316 F/g) [26], rGO/VOx nanosheets (635 F/g and 79.5 Wh/kg) [40], VOx nanoribbons/graphene (437 F/g) [41] and graphene/vanadium oxide free-standing monolith composites (358 F/g and 26.2 Wh/kg) [42]. These previous results are summarized in Table 2. It is worthy to notice that the capacitance values reported in this work correspond to solid state devices, which are flexible as demonstrated by the pictures in the inset of Fig. 2a. In contrast, the capacitance values reported in Table 2 correspond to VOx/graphene electrodes and were reported as “potentially useful” for SC devices. The electrochemical properties of the materials reported in Table 2 were obtained using a three electrodes configuration, therefore they are unfinished devices. Finally, the stability of the best device GSC-CNT/VO was analyzed through the curve of capacitance retention vs. cycle number, see Fig. S5 in supporting information. As observed, the capacitance of the GSC-CNT/VO device is maintained in the range of 96–100% during the first 70 cycles of charge/discharge. After 80 cycles, the capacitance is reduced to 88% and abruptly decreases to 66% after 150 cycles.

Table 1
Electrochemical characteristics of the graphene/V_2O_5-based flexible supercapacitors studied in this work.

Device	Specific capacitance (F/g)	Energy density (Wh/kg)
GSC	271	54.2
GSC-VOx	531	106.2
GSC-CNT/VOx	1848	369.6

Table 2
Electrochemical performance of graphene based SCs previously reported in literature.

Material	Specific capacitance (F/g)	Energy density (Wh/kg)	Reference
VO_x NWs/rGO	1002	116	[24]
VO_x nanobelts/graphene	288	—	[25]
rGO/VO_x nanoparticles	384	80.4	[23]
Nanoporous VO_x	316	—	[26]
rGO/VO_x nanosheets	655	79.5	[40]
VO_x nanoribbons/ graphene	437	—	[41]
Graphene/VO_x monolith composite	358	26.2	[42]

3.4. Charge storage mechanisms in VOx based flexible supercapacitors

The storage charge in the GSC-VOx device can be explained as follows: According to the literature, the reduction of VOx (a change in the oxidation state of neighboring vanadium atoms from V^{+5} to V^{+4} or lower valences) causes the formation of oxygen vacancies (VO) [43]. These vacancies (pairs of VO-V^{+4}) work as redox centers for producing electrochemical charges which will provide more migration paths for the fast positive ion diffusion, which in turn, delays the voltage discharge of SCs/batteries [44]. The presence of V^{4+} (after V^{+5} reduction) was confirmed by the cathodic peak centered at ≈0.45 V in the C-V curve of the GSC-VOx device (inset in Fig. 2c) and by the change of coloration from yellow to dark blue on the FGE + VOx electrode. The change of coloration was visually observed because the VOx was removed from the GSC-VOx device. Moreover, the formation of vacancies VO by chemical interactions of the FGE + VOx electrode with the gel electrolyte was confirmed by the absorbance spectrum of the FGE + VOx electrode. Such spectrum presented a broader and more intense absorbance band than that for the pure VOx powder, see pink and red curves in Fig. 3a. According to previous reports, the broadening and enhancement of the absorbance in the 250–400 nm region by VOx are typically associated with the formation of VO vacancies [45]. Thus, the presence of VO-V^{+4} redox centers on the anode electrode of the GSC-VOx device decreases the rate of current discharge, this in turn, stabilizes the voltage discharge, which remains at 0.14 V during 458 min.

Interestingly, the output voltage was 0.24 V higher for the GSC-CNT/VOx device and remained constant during 445 min, see Fig. 2d. To clarify the reason for the increment, absorbance, XPS and Raman measurements were performed for the FGE + CNT/VOx electrode after its use in the SC device. The absorbance spectrum of the FGE + CNTs electrode was obtained and a broad band from 200 to 600 nm was observed, see Fig. 3a. This figure shows shoulders centered at 260 nm and at 400 nm, which are associated to the π-π transitions in the CNTs and to oxygen vacancies in the CNTs [46], respectively. These vacancies were formed after functionalization of the CNTs [35]. When the FGE + CNT/VOx electrode interacts with the gel electrolyte, more oxygen vacancies are formed in VOx, therefore, the absorbance of the FGE + CNT/VOx electrode is broader than that for the FGE + CNTs electrode. In addition, Raman measurements corroborated the increase of vacancies on the FGE + CNTs electrode after the deposition of VOx on it. Since the I_D/I_G ratio (calculated with the intensities of the D and G bands in Fig. 3b) increases from 0.1 to 0.4. The I_D/I_G ratio increased because the intensity of the D band was higher. This band is typically associated to disordered carbon and defective rings in the CNTs [46]. XPS analysis was performed to find the chemical species on the FGE + CNTs and FGE + CNTs/VOx electrodes. Fig. 3c illustrates the deconvoluted XPS spectra for the O1s orbital corresponding to the FGE + CNTs electrode. Two peaks at 532.8 eV and 534.1 eV corresponding to the C═O, C-O, and COOH bonds [47,48], respectively, were observed. The deconvoluted XPS spectrum for the FGE + CNT-VOx electrode (O1s orbital) shows two

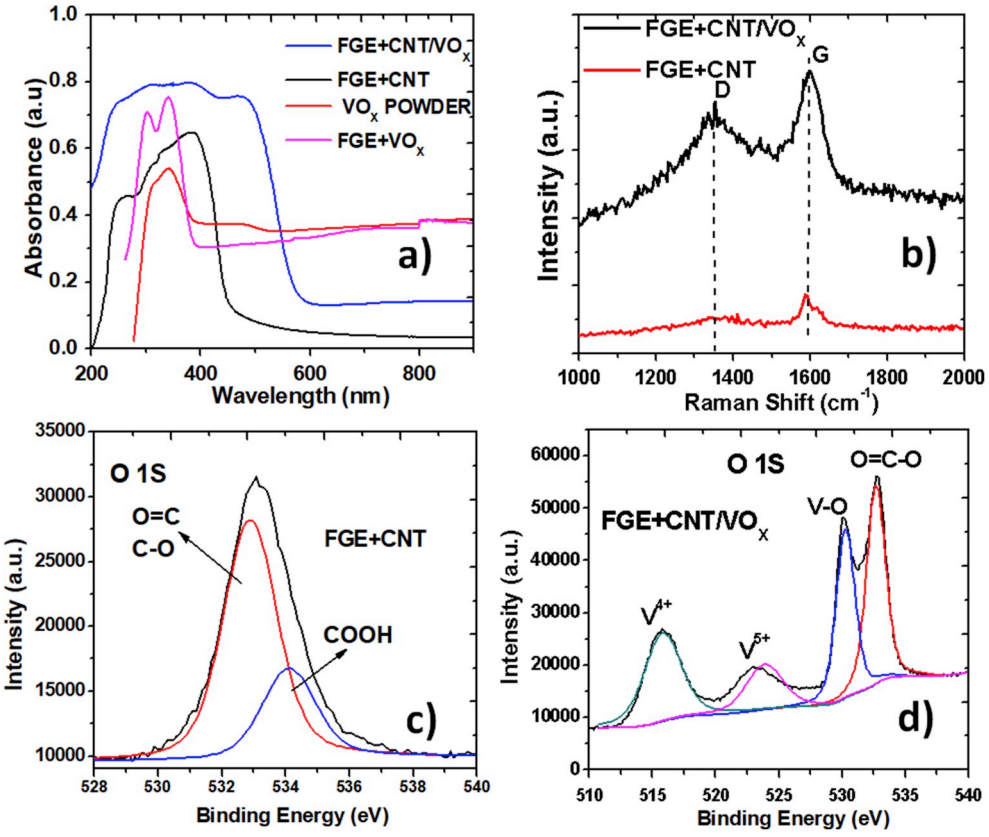

Fig. 3. Absorbance spectra of VOx powders, FGE + VOx, FGE + CNTs and FGE + CNTs/VOx electrodes; b) Raman spectra of FGE + CNT and FGE + CNTs/VOx electrodes; c) and d) are XPS spectra for the O 1s orbital in the FGE + CNT and FGE + CNTs/VOx electrodes.

bands at 530.1 eV and 532.8 eV, which correspond to the V-O and O-C═O bonds (see Fig. 3d), respectively. In addition, the other two bands at 515.7 eV and 524 eV were observed due to the V^{4+} and V^{5+} oxidation states [49], respectively. In fact, the reduction from V^{5+} to V^{4+} can be confirmed by the cathodic shoulder centered at 0.4 V (black curve in Fig. 2c), while the anodic shoulder at 0.26 V could be associated to the oxidation of CNTs or graphene. The absorbance spectra and XPS analysis demonstrated: i) the presence of carboxyl groups on CNTs (which produced oxygen vacancies); ii) the simultaneous presence of V^{4+} and V^{5+} on the surface of FGE + CNT/VOx electrode (V^{5+} was reduced to V^{4+} due to the chemical reaction of the gel electrolyte with the FGE + CNT/VOx electrode); and iii) the presence of oxygen vacancies in VOx. Thus, the V^{4+}-VO vacancies in VOx and defect sites in CNTs can act as redox centers [50,51] which donate electrons that can be quickly transported by the CNTs and graphene, this in turn, increasea the charge transfer rate and prolongs the discharge time in the GSC-CNT/VOx device with respect to the GSC-VOx device. Fig. 4a and b shows the Tauc plots for the FGE + CNT/VOx and FGE + VOx electrodes using the equations reported in Ref. [36]). The intersection of the linear part of the curve $(\alpha h\nu)^2$ vs. energy with the X-axis (see red doted lines in Fig. 4a) permits to estimate the bandgap energy value (E_g). The E_g values were 2.14 eV and 2.25 eV for the electrode with and without VOx, respectively. The lower E_g value obtained for the FGE + CNT/VOx electrode suggests better electrical conductivity. This will produce higher voltages and current densities in the GSC-CNT/VOx device compared with the GSC-VOx device, see Fig. 2c. Additionally, the CNTs provided extra surface area to the FGE, promoting a higher capacity for ion storage, which benefits the electrochemical performance of the GSC-CNT/VOx device.

The electrochemical impedance spectroscopy (EIS) was achieved to understand the charge transfer process in the devices and to determine the resistance associated with the charge storage at the electrode/electrolyte interface. EIS were achieved applying an AC voltage with 20 mV amplitude in the frequency range from 0.01 HZ to 100 KHz under open circuit potential conditions. The Nyquist plots in Fig. 5 exhibit two parts: a straight line in the low frequency region and a semi-circle in the high frequency region. The interception of the semi-circle with the X-axis gives equivalent series resistance (R_s), which is the inner resistance of the electrode and electrolyte and the diameter of the semi-circle provides the charge transfer resistance (R_{ct}) at the electrode/electrolyte interface [52,53]. From Fig. 5, the values for (R_s, R_{ct}) were (49 Ω, 131 Ω), (25 Ω, 75 Ω) and (31 Ω, 57 Ω) for the GSC, GSC-VOx and GSC-CNT/VOx devices, respectively. As observed, the introduction of VOx in the SCs decreased the internal series resistance from 49 Ω to 25 Ω and the charge transfer resistance from 131 Ω to 75 Ω, which enhanced the capacitance from 271 (GSC device) to 531 F/g (GSC-VOx device). If CNTs are also added to the SCs, the R_{ct} is reduced from 75 Ω (GSC-VOx device) to 57 Ω (GSC-CNT/VOx device), which increased even more the capacitance (from 531 to 1848 F/g). Decreasing both resistances was a key issue to increase the overall performance of the SCs, since it favors the diffusion of ions through the electrode/electrolyte interface for their storage, which in turn, benefited the capacitance.

4. Conclusions

This work reports the fabrication of flexible graphene SCs that contain VOx and CNTs in their electrodes (anodes). All the devices, except the device without VOx and CNTs, presented capacitive and constant voltage components. The capacitance values of flexible graphene SCs made with anodes that contained VOx and CNTs/VOx layers were 95% and 581% higher than that for the SC device made with an anode without these layers, respectively. The prolonged discharge time in the GSC-VOx device was favored by the presence of V^{4+}-VO vacancies in its anode, which acted as redox centers. In the case of the GSC-CNTs/VOx device, its anode contained not only V^{4+}-VO vacancies (redox centers) but also defects coming from the CNTs (which were produced on their surface by the treatment with nitric acid). This raises the voltage even more from 0.14 V to 0.38 V and the discharge time was longer. In addition, the presence of CNTs on the FGEs improved the current density of the SCs because they provided extra surface area for ion storage. The main advantage of our devices is the fact that they require only 10 s to be completely charged, which is lower than the charging times previously reported. The results presented here demonstrate that the strategies of: 1) functionalizing the CNT with carboxylic groups, 2) the chemical reduction of VOx, and 3) the deposition of VOx on the FGEs, produced SCs with prolonged discharge times which is suitable to increase their energy density. Hence, the results presented here could be useful to design SCs with high energy densities for mobile/portable applications.

Declaration of competing interest

The authors declare that they have no known competing financial interests or personal relationships that could have appeared to influence the work reported in this paper.

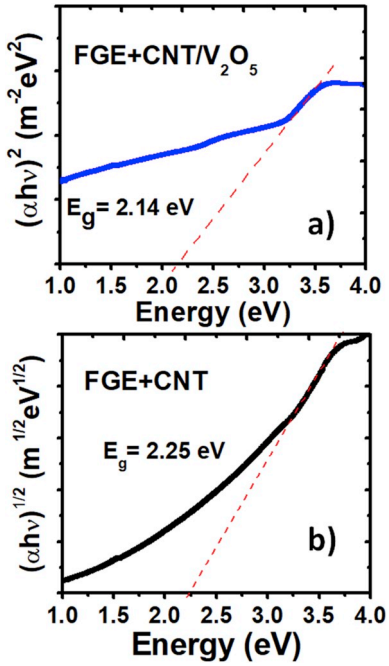

Fig. 4. Tauc plots for the: a) FGE + CNT, and b) FGE + CNTs/VOx electrodes.

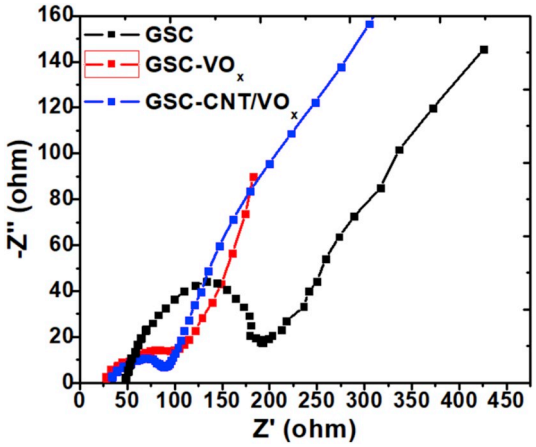

Fig. 5. EIS Nyquist plots for the GSC, GSC-VOx and GSC + CNTs/VOx devices.

Acknowledgments

We appreciate the financial support of the CONACYT-Catedras program. We also acknowledge the technical support from Ana Peña and Beatriz Rivera for SEM and XRD measurements in LINAN IPICYT. Additionally, we thank Wilian Cauich and LANNBIO (Cinvestav-Mérida) for the XPS measurements. Partial financial support of Welch Foundation of Texas (USA) grant AT-1617 is also highly appreciated.

Appendix A. Supplementary data

Supplementary data to this article can be found online at https://doi.org/10.1016/j.matchemphys.2020.122698.

References

[1] Z. Wang, H.H. Wu, Q. Li, F. Besenbacher, Y. Li, X.C. Zeng, M. Dong, Reversing interfacial catalysis of ambipolar WSe_2 single crystal, Adv. Sci. (2019) 1901382.
[2] X. Wang, Y. Chen, B. Yu, Z. Wang, H. Wang, B. Sun, W. Li, D. Yang, W. Zhang, Hierarchically Porous W-Doped CoP Nanoflake arrays as highly efficient and stable electrocatalyst for pH-universal hydrogen evolution, Small 15 (2019) 1902613.
[3] K. Chen, Q. Wang, Z. Niu, J. Chen, Graphene-based materials for flexible energy storage devices, J. Energy Chem. 27 (2018) 12–24.
[4] G.P. Pandey, T. Liu, E. Brown, Y. Yang, Y. Li, X.S. Sun, Y. Fang, J. Li, Mesoporous hybrids of reduced graphene oxide and vanadium pentoxide for enhanced performance in lithium-ion batteries and electrochemical capacitors, ACS Appl. Mater. Interfaces 8 (2016) 9200–9210.
[5] J. Wen, Y. Yu, C. Chen, A review on lithium-ion batteries safety issues: existing problems and possible solutions, Mater. Express. 2 (2012) 197–212.
[6] M.A. Bissett, I.A. Kinloch, R.A.W. Dryfe, Characterization of MoS_2 graphene composites for high-performance coin cell supercapacitors, ACS Appl. Mater. Interfaces 7 (2015) 17388–17398.
[7] H. Kim, K.Y. Park, J. Hong, K. Kang, All-graphene-battery: bridging the gap between supercapacitors and lithium ion batteries, Sci. Rep. 4 (2014) 1–8.
[8] Z. Wang, J. Liu, X. Hao, Y. Wang, Y. Chen, P. Li, M. Dong, Investigating the stability of molecule doped graphene field effect transistors, New J. Chem. 43 (2019) 15275–15279.
[9] X. Zang, Q. Chen, P. Li, Y. He, X. Li, M. Zhu, X. Li, K. Wang, M. Zhong, D. Wu H. Zhu, Highly flexible and adaptable, all-solid-state supercapacitors based on graphene woven-fabric film electrodes, Small 10 (2014) 2583–2588.
[10] M.H. Ervin, L.T. Le, Woo, Y. Lee, Inkjet-printed flexible graphene-based supercapacitor, Electrochim. Acta 147 (2014) 610–616.
[11] K. Gao, Z. Shao, J. Li, X. Wang, X. Peng, W. Wang, F. Wang, Cellulose nanofiber–graphene all solid-state flexible supercapacitors, J. Mater. Chem. 1 (2013) 63.
[12] I.L. Tsaia, J. Caob, L.l. Fevrea, B. Wang, R. Todd, R.A.W. Dryfe, A.J. Forsyth, Graphene-enhanced electrodes for scalable supercapacitors, Electrochim. Acta 257 (2017) 372–379.
[13] H. Li, Y. Tao, X. Zheng, J. Luo, F. Kang, H.M. Cheng, Q.H. Yang, Ultra-thick graphene bulk supercapacitor electrodes for compact energy storage, Energy Environ. Sci. 9 (2016) 3135.
[14] S. Zeng, H. Chen, F. Cai, Y. Kang, M. Chen, Q. Li, Electrochemical fabrication of carbon nanotube/polyaniline hydrogel film for all-solid-state flexible supercapacitor with high areal capacitance, J. Mater. Chem. 3 (2015) 23864–23870.
[15] T. Liu, J.J. Xu, Q.C. Liu, Z.W. Chang, Y.B. Yin, X.Y. Yang, X.B. Zhang, Ultrathin, lightweight, and wearable Li-O_2 battery with high robustness and gravimetric/volumetric energy density, Small 13 (2017) 1602952.
[16] G. Wu, P. Tan, D. Wang, Z. Li, L. Peng, Y. Hu, C. Wang, W. Zhu, S. Chen, W. Chen, High-performance supercapacitors based on electrochemical-induced vertical-aligned carbon nanotubes and polyaniline nanocomposite electrodes, Sci. Rep. 7 (2017) 43676.
[17] Y. Zhang, Y. Jiao, M. Liao, B. Wang, H. Peng, Carbon nanomaterials for flexible lithium ion batteries, Carbon 124 (2017) 79–88.
[18] D. Chen, R. Yi, S. Chen, T. Xu, M.L. Gordin, D. Lv, D. Wang, Solvothermal synthesis of V_2O_5/graphene nanocomposites for high performance lithium ion batteries, Mater. Sci. Eng. B 185 (2014) 7–12, https://doi.org/10.1016/j.mseb.2014.01.015.
[19] I. Mjejri, A. Rougier, M. Gaudon, Low-cost and facile synthesis of the vanadium oxides V_2O_2, VO_2, and V_2O_5 and their magnetic, thermochromic and electrochromic properties, Inorg. Chem. 56 (2017) 1734–1741.
[20] B. Park, S.M. Oh, Y.K. Jo, S.J. Hwang, Efficient electrode material of restacked Na-V_2O_5-graphene nanocomposite for Na-ion batteries, Mater. Lett. 178 (2016) 79–82.
[21] Q. Liu, Z.F. Li, Y. Liu, H. Zhang, Y. Ren, C.J. Sun, W. Lu, Y. Zhou, L. Stanciu, E. A. Stach, J. Xie, Graphene-modified nanostructured vanadium pentoxide hybrids with extraordinary electrochemical performance for Li-ion batteries, Nat. Commun. 6 (2015) 1–10.
[22] F. Maroni, A. Birrozzi, G. Carbonari, F. Croce, R. Tossici, S. Passerini, F. Nobili, Graphene/V_2O_5 cryogel composite as a high-energy cathode material for lithium-ion batteries, ChemElectroChem 4 (2017) 613–619.
[23] Z. Liu, H. Zhang, Q. Yang, Y. Chen, Graphene/V_2O_5 hybrid electrode for an asymmetric supercapacitor with high energy density in an organic electrolyte, Electrochim. Acta 287 (2018) 149–157.
[24] D.J. Ahirrao, K. Mohanapriya, N. Jha, V_2O_5 nanowires-graphene composite as an outstanding electrode material for high electrochemical performance and long-cycle-life supercapacitor, Mater. Res. Bull. 108 (2018) 73–82.
[25] M. Lee, S.K. Balasingam, H.Y. Jeong, W.G. Hong, H.B.R. Lee, B.H. Kim, Y. Jun, One-step hydrothermal synthesis of graphene decorated V_2O_5 nanobelts for enhanced electrochemical energy storage, Sci. Rep. 5 (2015) 1–8, https://doi.org/10.1038/srep08151.
[26] B. Saravanakumar, K.K. Purushothaman, G. Muralidharan, Interconnected V_2O_5 nanoporous network for high-performance supercapacitors, ACS Appl. Mater. Interfaces 4 (2012) 4484–4490.
[27] G. Xu, X. Wang, X. Chen, L. Jiao, Facile synthesis and phase transition of V_2O_3 nanobelts, RSC Adv. 5 (2015) 17782–17785.
[28] J. Oliva, A.I. Martinez, A.I. Oliva, R. Ochoa-Valiente, C.R. Garcia, Q. Pei, Flexible graphene composites with high thermal conductivity as efficient heat sinks for high power LEDs, J. Phys. D Appl. Phys. 52 (2019), 025103.
[29] Y.X. Qin, C. Liu, W.W. Xie, M.Y. Cui, Controllable synthesis of ultrathin vanadium oxide nanobelts via an EDTA-mediated hydrothermal process, Chin. Phys. B 25 (2016), 027307.
[30] X. Lepró, M.D. Lima, R.H. Baughman, Spinnable carbon nanotube forests grown on thin, flexible metallic substrates, Carbon 48 (2010) 3621–3627.
[31] B.P. Singh, V. Choudhary, S. Teotia, T.K. Gupta, V.N. Singh, S.R. Dhakate, R. B. Mathur, Solvent free, efficient, industrially viable, fast dispersion process based amine modified MWCNT reinforced epoxy composites of superior mechanical properties, Adv. Mater. Lett. 6 (2015) 104–113.
[32] S. Fang, M. Zhang, A.A. Zakhidov, R.H. Baughman, Structure and process-dependent properties of solid-state spun carbon nanotube yarns, J. Phys. Condens. Matter 22 (2010) 334221.
[33] A. Sayah, F. Habelhames, A. Bahloul, B. Nessark, Y. Bonnassieux, D. Tendelier, M. E. Jouad, Electrochemical synthesis of polyaniline-exfoliated graphene composite films and their capacitance properties, J. Electr. Chem. 818 (2018) 26–34.
[34] M.A. Atieh, O.Y. Bakather, B. Al-Tawbini, A.A. Bukhari, F.A. Abuilaiwi, M. B. Fettouhi, Effect of carboxylic functional group functionalized on carbon nanotubes surface on the removal of lead from water, Bioinorgan. Chem. Appl. 2010 (2010) 603978.
[35] S.K. Mishra, S.N. Tripathi, V. Choudhary, B.D. Gupta, Surface plasmon resonance-based fiber optic methane gas sensor utilizing graphene-carbon nanotubes-poly (methyl methacrylate) hybrid nanocomposite, Plasmonics 10 (2015) 1147–1157.
[36] M.M. Margoni, S. Mathuri, K. Ramamurthi, R.R. Babu, K. Sethuraman, Sprayed vanadium pentoxide thin films: influence of substrate temperature and role of HNO_3 on the structural, optical, morphological and electrical properties, Appl. Surf. Sci. 418 (2017) 280–290.
[37] A. Venkatesan, N.R. Krishna Chandar, A. Kandasamy, M. Karl Chinnu, K. N. Marimuthu, R. Mohan Kumar, R. Jayavel, Luminescence and electrochemical properties of rare earth (Gd, Nd) doped V_2O_5 nanostructures synthesized by a non-aqueous sol-gel route, RSC Adv. 5 (2015) 21778–21785.
[38] M. Liang, M. Zhao, H. Wang, J. Shen, X. Song, Enhanced cycling stability of hierarchical $NiCo_2S_4$@Ni$(OH)_2$@PPy core-cell nanotube arrays for aqueous asymmetric supercapacitors, J. Mater. Chem. 6 (2018) 2482–2493.
[39] H. Sun, A. Varzi, V. Pellegrini, D.A. Dinh, R. Raccichini, A.E. Del Rio-Castillo, M. Prato, M. Colombo, R. Cingolani, B. Scrosati, S. Passerini, F. Bonaccorso, How much does size really matter? Exploring the limits of graphene as Li ion battery anode material, Solid State Commun. 251 (2017) 88–93.
[40] D.H. Nagaraju, Q. Wang, P. Beaujuge, H.N. Alshareef, Two-dimensional heterostructures of V_2O_5 and reduced graphene oxide as electrodes for high energy density asymmetric supercapacitors, J. Mater. Chem. A. 2 (2014) 17146–17152.
[41] G. Ye, Y. Gong, K. Keyshar, E.A.M. Husain, G. Brunetto, S. Yang, R. Vajtai, P. M. Ajayan, 3D reduced graphene oxide coated V_2O_5 nanoribbon scaffolds for high-capacity supercapacitor electrodes, Part. Part. Syst. Char. 32 (2015) 817–821.
[42] L. Deng, Y. Gao, Z. Ma, G. Fan, Free-standing graphene/vanadium oxide composite as binder-free electrode for asymmetrical supercapacitor, J. Colloid Interface Sci. 505 (2017) 556–565.
[43] Q. Wang, M. Brier, S. Joshi, A. Puntambekar, V. Chakrapani, Defect-induced Burstein-Moss shift in reduced V_2O_5 nanostructures, Phys. Rev. B 94 (2016) 1–12.
[44] Y. Sun, Z. Xie, Y. Li, Enhanced lithium storage performance of V_2O_5 with oxygen vacancy, RSC Adv. 8 (2018) 39371–39376.
[45] Q. Wang, M. Brier, S. Joshi, A. Puntambekar, V. Chakrapani, Defect-induced Burstein-Moss shift in reduced V_2O_5 nanostructures, Phys. Rev. B 94 (2016) 1–12.
[46] R.A. Morales, C.F. Matos, E.G. Castro, W.H. Schreiner, M.M. Oliveira, A.J. G. Zarbin, The effect of different chemical treatments on the structure and stability of aqueous dispersion of iron- and iron oxide-filled multi-walled carbon nanotubes, J. Braz. Chem. Soc. 22 (2011) 2191–2201.
[47] J.P. Boudou, J.I. Paredes, A. Cuesta, A. Martínez-Alonso, J.M.D. Tascón, Oxygen plasma modification of pitch-based isotropic carbon fibers, Carbon 41 (2003) 41–56.
[48] S. Sali, H.R. Mackey, A.A. Abdala, Effect of graphene oxide synthesis method on properties and performance of polysulfone-graphene oxide mixed matrix membranes, Nanomaterials 9 (2019) 769.
[49] G. Huang, C. Li, X. Sun, J. Bai, Fabrication of vanadium oxide, with different valences of vanadium, -embedded carbon fibers and their electrochemical performance for supercapacitor, New J. Chem. 41 (2017) 8977–8984.
[50] Z. Lv, J. Zhang, Y. Lv, Y. Cheng, S.P. Jiang, Y. Xiang, S. Lu, The electrocatalytic characterization and mechanism of carbon nanotubes with different numbers of

walls for the VO_2^+/VO^{2+} redox couple, Phys. Chem. Chem. Phys. 20 (2018) 7791–7797.
[51] D.Z.W. Tan, H. Cheng, S.T. Nguyen, H.M. Duong, Controlled synthesis of MnO2/CNT nanocomposites for supercapacitor applications, Mater. Technol. 9 (2014) A107–A113.
[52] S. Kaipannan, S. Marappan, Fabrication of 9.6 V high-performance asymmetric supercapacitors stack based on nickel hexacyanoferrate-derived Ni(OH)2 nanosheets and bio- derived activated carbon, Sci. Rep. 9 (2019) 1–14.
[53] H. Cheng, A.D. Su, S. Li, S.T. Nguyen, L. Lu, C.Y.H. Lim, H.M. Duong, Facile synthesis and advanced performance of Ni(OH)2/CNTs nanoflake composites on supercapacitor applications, Chem. Phys. Lett. 601 (2014) 168–173.